

Evolution of the mosaic structure in InGaN layer grown on a thick GaN template and sapphire substrate

Engin Arslan · Mustafa K. Ozturk ·
Huseyin Çakmak · Pakize Demirel ·
Süleyman Özçelik · Ekmel Ozbay

Received: 8 April 2013 / Accepted: 29 July 2013 / Published online: 8 August 2013
© Springer Science+Business Media New York 2013

Abstract The $\text{In}_x\text{Ga}_{1-x}\text{N}$ epitaxial layers, with indium (x) concentration changes between 0.16 and 1.00 (InN), were grown on GaN template/(0001) Al_2O_3 substrate by metal organic chemical vapour deposition. The indium content (x), lattice parameters and strain values in the InGaN layers were calculated from the reciprocal lattice mapping around symmetric (0002) and asymmetric (10–15) reflection of the GaN and InGaN layers. The characteristics of mosaic structures, such as lateral and vertical coherence lengths, tilt and twist angle and heterogeneous strain and dislocation densities (edge and screw dislocations) of the InGaN epilayers and GaN template layers were investigated by using high-resolution X-ray diffraction (HR-XRD) measurements. With a combination of Williamson–Hall (W-H) measurements and the fitting of twist angles, it was found that the indium content in the InGaN epilayers did not strongly effect the mosaic structures' parameters, lateral and vertical coherence lengths, tilt and twist angle, or heterogeneous strain of the InGaN epilayers.

1 Introduction

III-Nitride semiconductors have attracted great interest in the past years for many applications in commercial devices [1, 2]. They have been used in optoelectronic devices, such as blue/ultraviolet (UV) lasers, light emitting diodes (LEDs), modulation-doped field effect transistors (MODFETs), metal-semiconductor field effect transistors (MESFETs), photodetectors, and high temperature/high power electronic devices [1–5]. Alloy band-gap energies adjustable from 0.7 to 6.2 eV at room temperature can be achieved by suitable alloy combinations in the InGaN, AlInN, and AlGaIn systems from which heterojunctions can be fabricated [2–5]. Because of the broad alloy band-gap energies' tunability of the InGaN, from near 0.7 up to 3.4 eV, it has been widely used as active layers for high-efficiency blue and green LED and laser diodes [2–5]. In addition, its highly tunable band-gap, high heat capacity, and low sensitivity to ionizing radiation properties make the InGaN alloys a suitable material for the solar energy industry [6]. However, it is a challenging task to grow high-quality InGaN, especially for higher concentrations of In in the ternary film (>20 %), which is a few 100 nm thick, and has been less successful [7, 8].

It is well known that the growth conditions of InGaN and GaN based alloys can significantly affect its optical, structural, and electrical characteristics [7, 8]. The slight adjustment of the growth parameters could lead to a large variation in the quality of the InGaN layer; therefore, an understanding of the growth kinetics of InGaN is of great importance, and this, eventually, may help to develop and fabricate better quality InGaN [7]. There are two main reasons for the limited success; the first is the degradation of the crystal quality of the InGaN layer due to the lattice mismatch between the underlying GaN template, substrate, and InGaN layer. There are still no widely available lattice

E. Arslan (✉) · H. Çakmak · P. Demirel · E. Ozbay
Department of Physics, Nanotechnology Research
Center-NANOTAM, Bilkent University, 06800 Ankara, Turkey
e-mail: engina@bilkent.edu.tr

E. Arslan · H. Çakmak · P. Demirel · E. Ozbay
Department of Electrical and Electronics Engineering,
Nanotechnology Research Center-NANOTAM,
Bilkent University, 06800 Ankara, Turkey

M. K. Ozturk · S. Özçelik
Department of Physics, Faculty of Science and Arts,
Gazi University, Teknikokullar, 06500 Ankara, Turkey

matched GaN substrates for the growth of wurzite GaN. The lattice mismatch between the GaN and sapphire (Al_2O_3), silicon carbide (SiC), and silicon (Si) substrates causes extended defects in *c*-axis oriented GaN grown including threading dislocations (TDs), stacking faults bounded by Shockley and Frank partial dislocations, and inversion domains are commonly observed [7–13]. The other reason limiting the structural quality is the tendency of thicker InGaN to phase segregate into In-rich and Ga-rich alloy regions during the deposition process, especially as the indium fraction increases [7]. Because of native point defects and a high *n*-type background carrier concentration, the InGaN alloys have an extreme affinity to being the doped *n*-type, which results in a big problem of *p* type doping InGaN alloys [7].

A mosaic model is widely used to describe the microstructure of the GaN based semiconductor materials that can be characterized by means of lateral and vertical coherence lengths (average size of the mosaic blocks) tilt and twist angle, heterogeneous strain and dislocation densities (edge and screw dislocations) [9, 10, 14–20]. The tilt describes the rotation of the mosaic blocks out-of the growth plane, and the twist in their in-plane rotation. The average absolute values of the tilt and twist are directly related with the full width at half maximum (FWHM) of the corresponding distributions of the crystallographic orientations [9, 10, 15, 17, 20]. The mosaic model of the crystals has been applied several times to GaN epilayers [9, 10, 15–28].

In this study, we grew $\text{In}_x\text{Ga}_{1-x}\text{N}$ layers on GaN/sapphire structures with different indium contents (*x*). The In contents (*x*) of the samples changed to 0.16, 0.21, 0.23, 0.52, 0.69, 0.78, 0.82, 0.89 and 1.00 (InN). The aim of the work presented here is to grow InGaN layers on a GaN template with a wide range of indium contents ($0.16 \leq x \leq 1.0$) and investigate the mosaic structure parameters of the GaN template layers and InGaN epilayers. For this purpose, the mosaic structure features (such as lateral and vertical coherence lengths, tilt and twist angle and heterogeneous strain) and dislocation densities (edge and screw dislocations) of hexagonal InGaN epilayers and GaN template layers were determined by high-resolution X-ray diffraction (HR-XRD) measurements. Additionally, atomic force microscopy (AFM) imaging was performed in order to obtain detailed knowledge on the surface morphology of the samples.

2 Experimental procedure

Epitaxial $\text{In}_x\text{Ga}_{1-x}\text{N}$ ($0.16 \leq x \leq 1.00$) layers were grown on double-polished 2-inch diameter sapphire (Al_2O_3) substrates in a low pressure metal organic chemical vapour deposition (MOCVD) reactor (Aixtron 200/4 HT-S) by using

trimethylgallium (TMGa), trimethylaluminum (TMAI), trimethylindium and ammonia as Ga, Al, In and N precursors, respectively. Prior to epitaxial growth, Al_2O_3 substrate was annealed at 1,120 °C for 15 min in order to remove surface contamination. The buffer structures of the all the samples consisted of a 10 nm thick, low-temperature (705 °C) GaN nucleation layer, and high temperature (1,100 °C) 2.3 μm GaN template layer. And nominally 150 nm undoped InGaN layer was grown on GaN template layer (Fig. 1a). The average InGaN layer thickness determined by scanning electron microscopy (SEM) was given in Fig. 1b. In this study, nine different samples were grown, with a different indium concentration, on GaN template layers. The In content was changed by changing the growth temperature and $\text{TMIn}/(\text{TEGa} + \text{TMin})$ ratio. The growth temperatures and the $\text{TMIn}/(\text{TEGa} + \text{TMin})$ ratio of the samples are 730, 745, 705, 580, 550, 550, 550, 550 °C and 0.40, 0.75, 0.79, 0.82, 0.87, 0.91, 0.95, and 1.00 for an indium content (*x*) of 0.16, 0.21, 0.23, 0.52, 0.69, 0.78, 0.82, 0.89 and 1.00 (InN), respectively. The samples were identified with consideration of the indium content as samples A, B, C, D, E, F, G, H, and K, 0.16, 0.21, 0.23, 0.52, 0.69, 0.78, 0.82, 0.89 and 1.00 (InN), respectively.

The crystalline quality of the GaN layers was examined by HR-XRD. The X-ray diffraction (XRD) was performed using a Bruker D-8 high-resolution diffractometer system, delivering $\text{CuK}\alpha 1$ (1.540 Å) radiation, using a prodded mirror, and 4-bounce Ge(220) symmetric monochromator. Data were collected on the symmetric (0002), (0004), (0006) and asymmetric (10–15), (20–22), (12–31), (10–11), (10–13), and (11–24) reflections as reciprocal space mappings (RSMs) or just ω and $\omega - 2\theta$ scans. The surface morphology was characterized by AFM.

3 Results and discussion

The surface morphology of the InGaN layers grown on GaN template layers is characterized by AFM. The root-mean-square (RMS) roughness is between 0.5 (for sample B) and 31.2 nm (for sample E). Figure 2a–d shows a comparison of the surface morphology for samples A, B, C, D, and E, respectively. Samples B and C have a smooth surface with low rms roughness (rms = 0.5 and 0.8 nm, respectively) compared to the other samples. The variation of the RMS roughness with indium content (*x*) in an InGaN layer is shown in Fig. 3. Based on the observation from the graph, the RMS roughness values of the InGaN layers did not show any systematic dependence on the indium content, but bigger rms values that were obtained for higher indium content include InGaN samples.

X-ray diffraction was performed for all of the samples to investigate the crystal phase of the InGaN epilayer on GaN

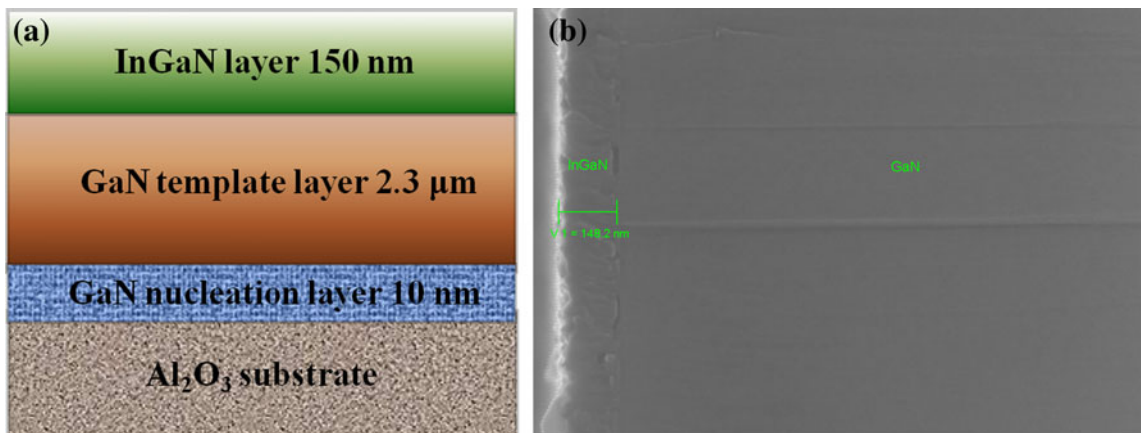


Fig. 1 a Schematic drawing and b SEM image of the InGaN/GaN/Al₂O₃ structures

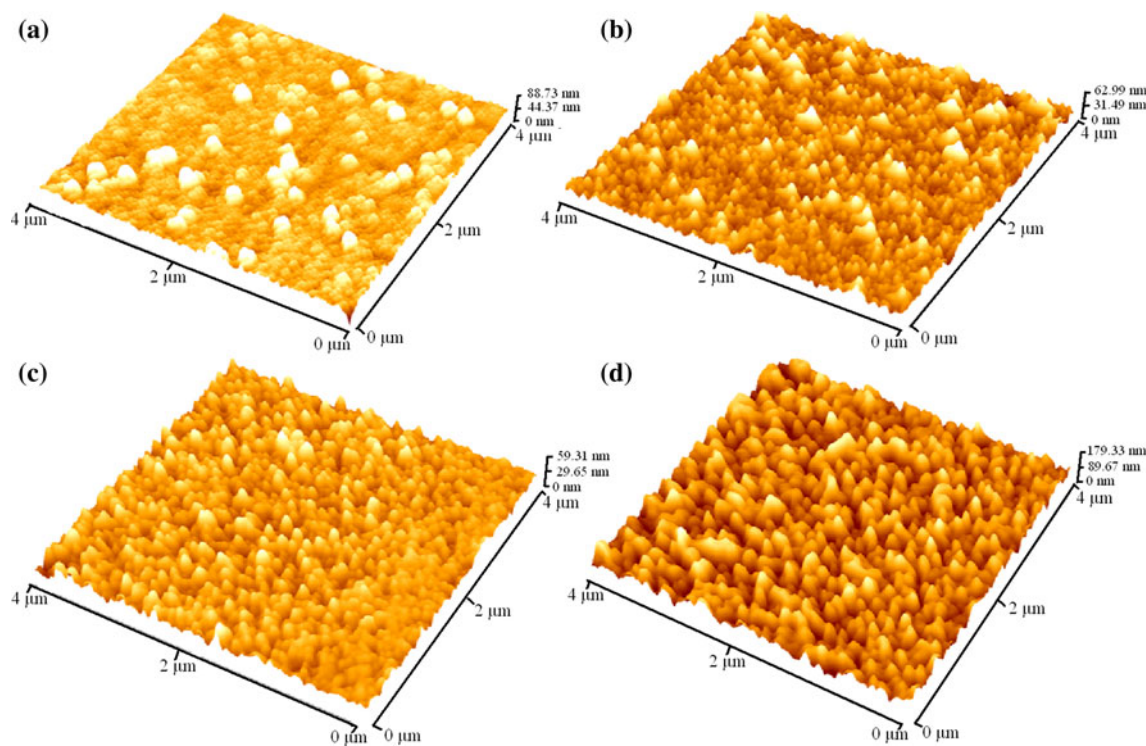


Fig. 2 AFM images ($4 \times 4 \mu\text{m}^2$ scans) of InGaN layers in a sample A, b sample D, c sample G and d sample K

template layer. Figure 4 shows the 2θ -scan XRD pattern of an InGaN epitaxial layer. The diffraction patterns exhibited the (0002) peaks of the wurtzite InGaN epilayers with different indium concentration are clearly observed at 31.35° , 31.52° , 31.76° , 31.90° , 32.17° , 32.90° , 33.67° , 33.77° , and 33.97° for sample A, B, C, D, E, F, G, H, and K, respectively. On the other hand, the (0002) peaks of the wurtzite GaN template layers were measured at similar angle values for all the samples at 34.56° .

An in-plane Φ -scan was also taken by rotating the sample around its surface normal direction to investigate

the in-plane alignment of InGaN epilayers. Figure 5 shows the Φ -scan pattern of the (10–15) plane of sample B. As seen in Fig. 5, the diffraction peaks from the (10–15) plane of InGaN were observed at $\sim 60^\circ$ intervals, confirming the hexagonal structure of the InGaN epilayer.

X-Ray RSM of the samples around symmetric and asymmetric reflection is a powerful tool to investigate the lattice parameters a and c , and thus to simultaneously determine the residual strain and stress as well as the exact alloy composition of the layers [29–33]. The lattice parameter a and c can be determined by XRD directly from

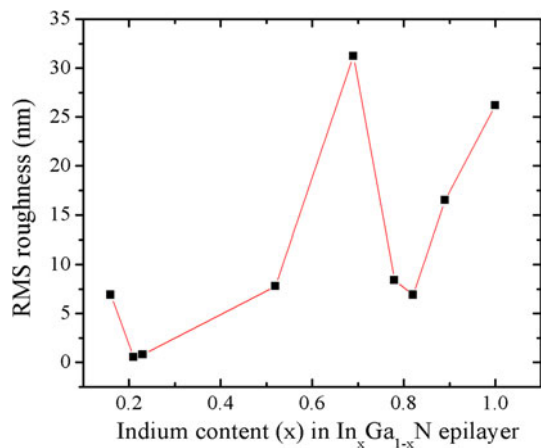


Fig. 3 Indium content dependence of the root-mean-square (RMS) roughness values for all samples

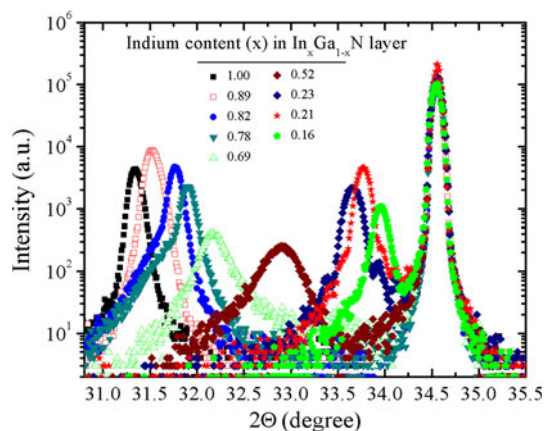


Fig. 4 The XRD pattern of the InGaN/GaN/sapphire samples

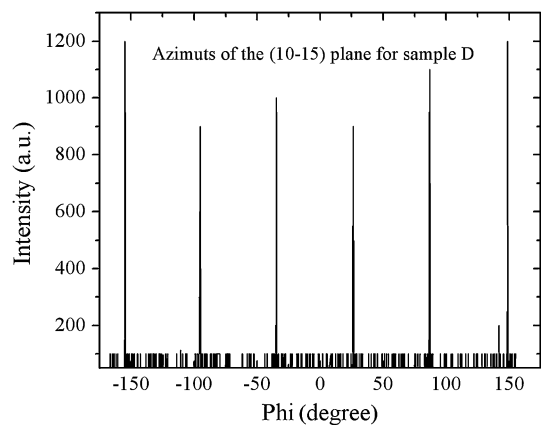


Fig. 5 Phi scan curve of asymmetric InGaN (10–15) reflection plane for sample D. Every peak shows azimuths of the (10–15) plane. The diffractive peak repeats every $\sim 60^\circ$

the hkl reflections in the symmetric $\omega - 2\theta$ scan by combining Bragg's equation $d_{hkl} = n\lambda/2\sin(\theta)$, where hkl is the Miller index in (hkl) notation, θ is the Bragg angle and λ is the wavelength of the X-rays, with the expression

for interplanar spacing in hexagonal structures given by [29–33]

$$\left(\frac{1}{d_{hkl}}\right)^2 = \frac{4h^2 + k^2 + hk}{3a^2} + \frac{l^2}{c^2}. \quad (1)$$

There are two unknowns (a and c), so at least two reflections measurements are needed. Usually, one or two high-angle symmetric reflections are measured from the (0002) and/or (0004) planes, from which c can be found directly [29]. In order to determine the a values, additionally, one or two high-angle asymmetric reflections measurement are needed (typically (10–15), (20–25) or (20–24) reflection). From high-angle asymmetric reflections a is determined with using the value of c found previously [29].

Because of the lattice and thermal mismatch between the substrate and III-nitrides, group-III-nitride alloy films are not grown directly on substrates (for example SiC, Al_2O_3 and Si as a substrate). In order to improve the crystalline quality, GaN layer used as a buffer layer [9]. Between the group-III-nitride alloy film and the GaN buffer, a nearly perfect in-plane orientation is established. In order to determine the strain and composition of the layer, commonly a peak from another III-nitride layer is used as the 'substrate' [29, 30]. If the material is assumed to be unstrained, then composition is the only factor affecting the lattice parameters and only lattice parameters needs to be measured. Vegard's law applies, which states that the lattice parameters of an alloy will vary linearly between the end members. For the c and a lattice parameter of InGaN (where x is the mole fraction of InN), this is given by [29–31]

$$c_0^{\text{InGaN}} = (1-x)c_0^{\text{GaN}} - xc_0^{\text{InN}} \quad (2)$$

$$a_0^{\text{InGaN}} = (1-x)a_0^{\text{GaN}} - xa_0^{\text{InN}}. \quad (3)$$

If both lattice parameter a and c are known, the sample strain can be taken into account in estimates of the composition. From the definition of Poisson's ratio, we find

$$\frac{[c_{\text{InGaN}} - c_0(x)]}{c_0(x)} = -2 \frac{C_{13}(x)}{C_{33}(x)} \frac{[a_{\text{InGaN}} - a_0(x)]}{a_0(x)}. \quad (4)$$

Where c_{InGaN} and a_{InGaN} are the measured lattice parameters, c_0 and a_0 are the relaxed parameters predicted by Vegard's law, and $C_{13}(x)$ and $C_{33}(x)$ are elastic constants linearly interpolated from the binary values. Poisson's ratio for a hexagonal crystal system biaxially strained perpendicular to (0001) is given by,

$$\nu = 2 \frac{C_{13}(x)}{C_{33}(x)}. \quad (5)$$

The linear relationship for the Poisson's ratio as a first-order approximation given is given by,

$$\nu_{\text{InGaN}} = (1-x)\nu_{\text{GaN}} + x\nu_{\text{InN}}. \quad (6)$$

Substitution of a_0^{InGaN} , c_0^{InGaN} and ν_{InGaN} in Eq. (4) obtained a cubic equation for x given below,

$$Kx^3 + Lx^2 + Mx^2 + N = 0. \tag{7}$$

The coefficient (K, L, M, N) of the Eq. (7) can be obtained by straightforward calculus. The solution of the Eq. (7) gives the In mole fraction x in the case of $In_xGa_{1-x}N$. There are three real solutions, but only one physically meaningful value of x in the interval $0 \leq x \leq 1$. By using calculated mole fraction x , in Eqs. (2), (3) and (6), the relaxed lattice parameters of the $InGaN$ alloy film a_0^{InGaN} and c_0^{InGaN} , as well as Poisson's ratio ν_{InGaN} can be obtained. In addition to the measured lattice parameters, the relaxed lattice constants of the GaN ($c_0^{GaN} = 0.51850$, $a_0^{GaN} = 0.31892$ nm) [29–31]) and the InN ($c_0^{InN} = 0.57033$, $a_0^{InN} = 0.35378$ nm) [29–31] and the elastic constant ($C_{13} = 103$ and $C_{33} = 405$ GPa) for GaN and ($C_{13} = 92$ and $C_{33} = 224$ GPa) InN [31, 34] are used as a input parameters in order to perform the calculations.

The strain components in the $InGaN$ layer ϵ_{zz} and ϵ_{xx} are defined as $\epsilon_{zz} = [c_{meas}^{InGaN} - c_0] / c_0$ and $\epsilon_{xx} = [a_{meas}^{InGaN} - a_0] / a_0$, where c_{meas}^{InGaN} and a_{meas}^{InGaN} are the measured lattice parameters, while c_0 and a_0 are the relaxed parameters given by Vegard's law [29, 30].

The RSM was examined for both symmetric (0002) and asymmetric (10–15) reflections of the GaN and $InGaN$ layers. The $\omega - 2\theta$ HR-XRD RSM of the (0002) (Fig. 6) and (10–15) (Fig. 7) reflections of the $InGaN/GaN(0001)/Al_2O_3$ samples are shown. The $R = 0$ and $R = 1$ lines are shows the calculated locations of the fully strained and the fully relaxed $InGaN$ layers of varying In content in Fig. 7. As can be seen the RSM of the (10–15) reflections, the $InGaN$ layers grown on GaN template layer are fully strained. The indium content (x), lattice parameters and strain values in the $InGaN$ layers were calculated from the reciprocal lattice mapping (RSM) around symmetric (0002) and asymmetric (10–15) reflection of the GaN and $InGaN$ layers, which values are given in Table 1.

$InGaN$ epilayers having a large lattice mismatch with respect to the GaN template layers and substrate form a mosaic structure of slightly misoriented subgrains, which is characterized by the nucleation of slightly misoriented islands and the coalescence of these islands toward a smooth surface [9–11, 15–21]. The mosaic blocks can be defined as slightly misoriented with respect to each other. The vertical and lateral correlation lengths, heterogeneous strain, and degree of mosaicity expressed by the tilt and twist angles are important parameters in characterizing the quality of the epitaxial films [9, 10, 15–21, 23–28]. The out-of-plane rotation of the blocks perpendicular to the surface normal is the mosaic tilt, and the in-plane rotation around the surface normal is the mosaic twist [9, 10, 15–21, 23–28]. The average absolute values of the tilt and twist are

directly related to the FWHM of the corresponding distributions of crystallographic orientations [15–21]. The parameters, lateral and vertical coherence length, tilt angle and heterogeneous strain along the c -axis, can be obtained from the Williamson–Hall (W–H) measurement, and the twist angle from approaches that were proposed by Srikant et al. [17] and Sun et al. [28] or from direct measurement [18, 19].

Each contribution to the broadening of particular XRD curves can be separated in a W–H measurement [14, 15]. Specifically in triple-axis diffractometer measurements, the broadening of the rocking curve (angular-scan or ω -scan) of the symmetric (0002), (0004), and (0006) reflections for the epitaxial layer is influenced only by the tilt angle α_{ilt} and short coherence length parallel to the substrate surface $L_{||}$ [9, 10, 14, 15, 20].

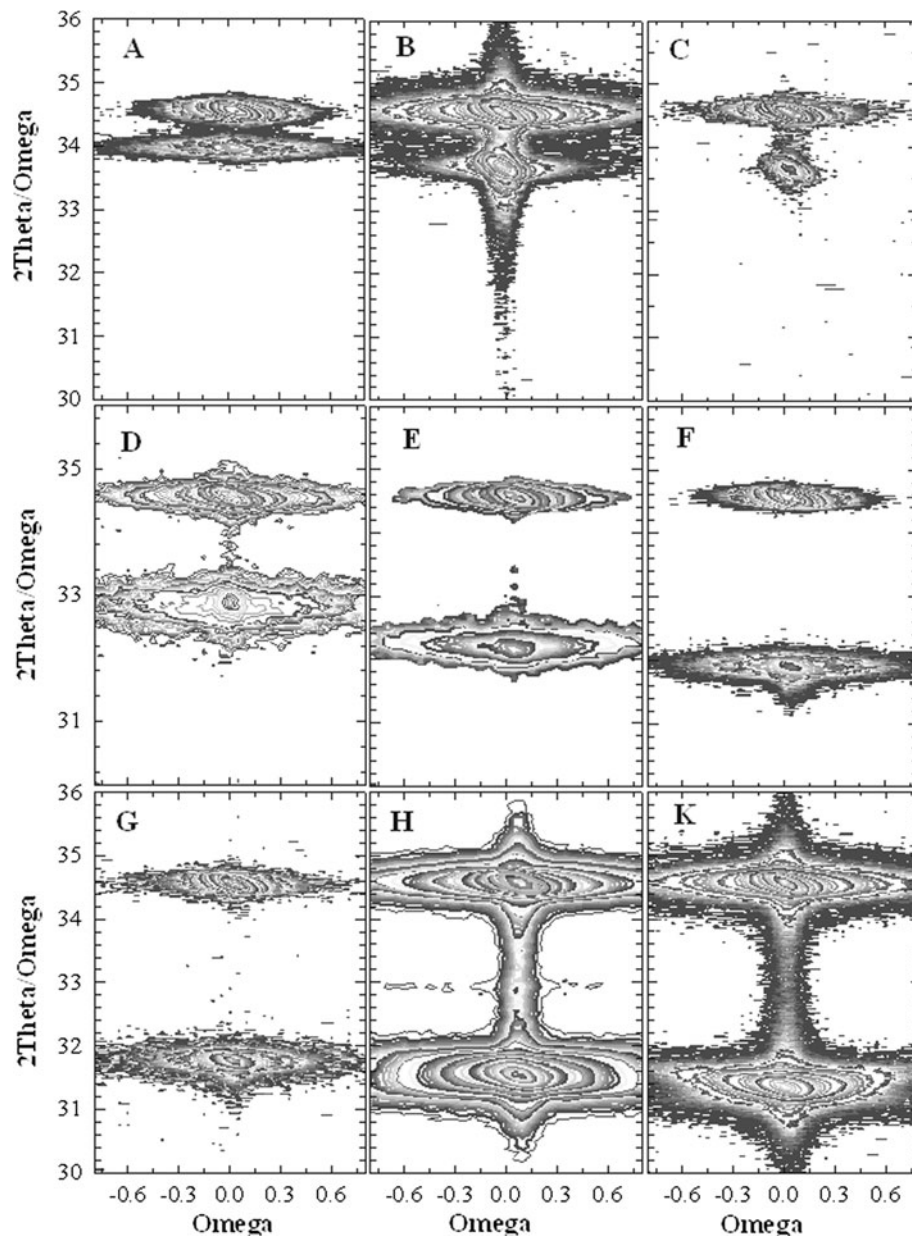
In the W–H plot, the $(FWHM)_{\omega}(\sin \theta) / \lambda$ is plotted against $(\sin \theta) / \lambda$ for each reflection and fitted by a straight line. Then, the mean tilt angle (α_{ilt}) is obtained from the slope of the linear dependence, and the lateral coherence length ($L_{||} = 0.9 / (2y_0)$) from the inverse of the y -intersection y_0 of the fitted line with the ordinate. Where $(FWHM)_{\omega}$ is in the angular unit, θ is the Bragg reflection angle, and λ is the X-ray wavelength.

In the radial-scan direction ($\omega - 2\theta$ scan) of the symmetric reflections, a small vertical correlation length and a heterogeneous strain along the c -axis causes a broadening of the Bragg reflections. These two parameters L_{\perp} and ϵ_{\perp} can similarly be derived from the W–H plot. In the W–H plot, $(FWHM)_{\omega-2\theta}(\cos \theta) / \lambda$ is plotted against $(\sin \theta) / \lambda$ for each reflection and again fitted by a straight line. From the y -intersection y_0 the vertical correlation length L_{\perp} can be calculated ($L_{||} = 0.9 / (2y_0)$) and the heterogeneous strain ϵ_{\perp} can be estimated directly from the slope of the line which is $4\epsilon_{\perp}$.

The W–H plots for symmetric plane reflections of the $InGaN$ epilayers and GaN template layers were done for the triple-axis ω - and $\omega - 2\theta$ -scan. Figure 8 shows the corresponding W–H plots of the $InGaN$ epilayers for the triple-axis (a) ω -scan and (b) $\omega - 2\theta$ -scan. The straight lines are linear fits to the experimental data. The expected linear behavior of the graphs is experimentally well confirmed, which gives the rather accurate tilt angle values.

The $L_{||}$ and α_{ilt} of the $InGaN$ epilayers and GaN template layers are shown in Table 2. The mean tilt angles' values of the samples change between the 1.0×10^{-3} and 18×10^{-3} degree. As seen, the mean tilt angles of the GaN template layers for all the samples, except sample K, were similar to each other and rather small. It can be seen in this table that the mean tilt angle for the sample K is the bigger than other samples. This difference can be attributed to the growth process. On the other hand, the mean tilt angles of

Fig. 6 Reciprocal space maps for the (0002) reflections of the three InGaN/GaN layers with increasing indium content

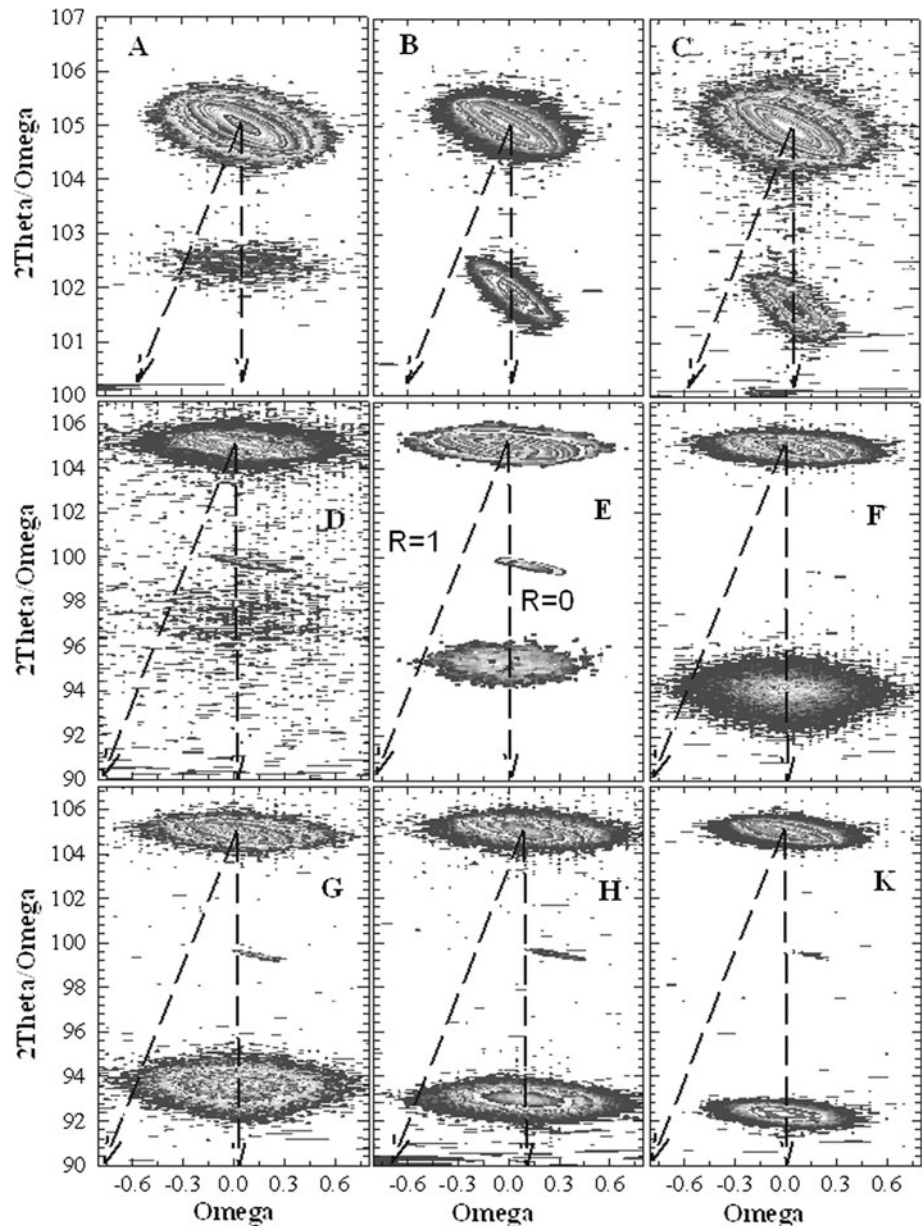


the InGaN epilayers are changes between the 0.3×10^{-3} (sample E) and 35×10^{-3} degree (sample D). Based on the observation of the measured mean tilt angles, there is not any systematic behavior between the tilt angle and indium content in InGaN epilayers (Fig. 9a). Furthermore, the indium content ratio in the InGaN epilayers does not affect the tilt angles of the mosaic blocks of the InGaN layers. The L_{\parallel} of the GaN template layers were determined to range from 10.5 to 6,432 nm. As can be seen in Table 2, the maximum values were observed for sample D and the minimum values obtained for sample K (InN epilayer). However, the L_{\parallel} , that was measured for the InGaN epilayers, has values ranging from 16.1 to 643 nm, and are smaller than the measured L_{\parallel} for GaN template layers.

The measured vertical coherence lengths, L_{\perp} , values for GaN template layers and InGaN epilayers are shown in Table 2. The L_{\perp} values for GaN template layers and InGaN epilayers range from 26.5 (sample A) to 45.0 nm (sample E) and 10.0 (sample A) to 56.2 nm (sample B), respectively. The ε_{\perp} values that were calculated for the GaN template layers and InGaN epilayers for all samples are shown in Table 2. The maximum ε_{\perp} values in the InGaN epilayers were obtained for sample E.

Generally, the mean twist angle (α_{twist}) between the subgrains of InGaN and GaN epilayers can be determined from the FWHM of ω -scan or Φ -scan XRD curves [9, 10, 15–20]. The mean twist angle can be extrapolated from a fit to the measured double-axis scans data for different (hkl)

Fig. 7 Reciprocal space maps for the (10–15) reflections of the three InGaN/GaN layers with increasing indium content. The lines connecting the fully strained to the fully relaxed *dashed lines* indicate the calculated relaxation directions in the reciprocal space for various InN mole fractions



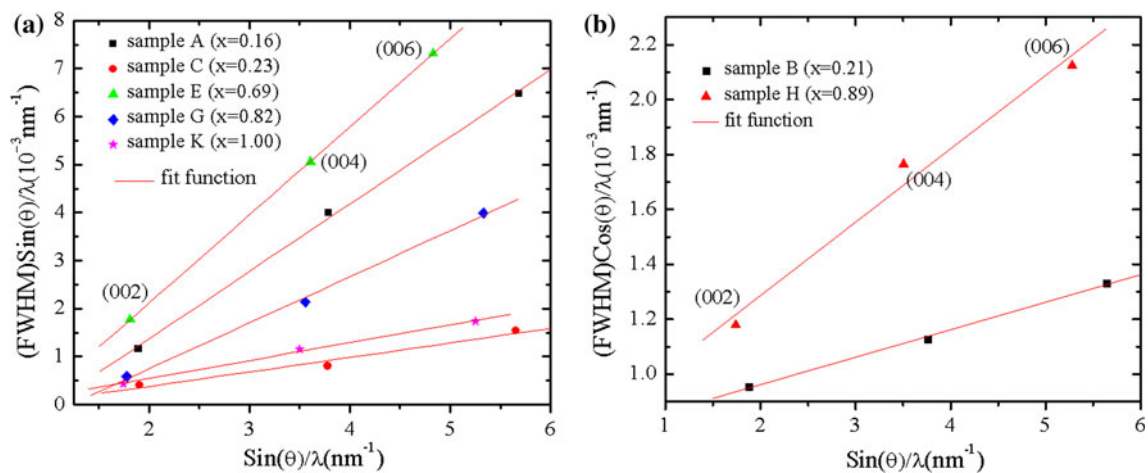
reflections in a skew symmetric diffraction. Several extrapolation and direct measurements methods have been reported in the literature for a mean twist angle calculation [15, 17, 18, 23, 24, 28]. Srikant et al. [17] and Sun et al. [28] proposed a geometrical model that considers the simultaneous presence of tilt and twist to fit the data from the measurement of ω -scans in skew geometry from reflections with increasing lattice plane inclination. Actually, these authors obtained the twist angle by the complicated calculation and fitting method. Metzger et al. [15] just used the FWHM of Φ -scan for (10–15) reflection to measure the twist angle. On the other hand, some authors [18, 19] proposed a simple empirical approach to obtain the mean twist angle directly without falling into complicated

computation and fitting procedure. In the other measurement method, a grazing incidence in-plane X-ray diffraction (GIIXD) technique was used, but in this technique a high intensity X-ray source such as a synchrotron and/or special X-ray optics is necessary [24, 25].

The FWHM of the rocking curve of an imperfect film is composed of several contributions, such as the mean tilt, twist, the average size of the sub-grains, and the inhomogeneous strain distributions. Although the broadening, due to a limited domain size and inhomogeneous strain, can be significant in highly imperfect films, their effects have been eliminated by using a slit of 0.6 mm that is placed in front of the detector in double-axis ω -scans. Indeed, their contribution to the overall broadening was found to be of

Table 1 The calculated In content (x), the lattice parameters a_{meas} and c_{meas} , the relaxed parameters c_0 and a_0 , calculated by using Vegard's law, strain components ε_{zz} and ε_{xx} and Poisson constant of the InGaN layers measured from the RSM

Sample ID	Indium content (x)	GaN template layers		InGaN layers						
		a_{meas} (nm)	c_{meas} (nm)	a_{meas} (nm)	c_{meas} (nm)	a_0 (nm)	c_0 (nm)	$\varepsilon_{zz} (\times 10^{-2})$	$\varepsilon_{xx} (\times 10^{-2})$	Poisson ratio
A	0.16	0.51842	0.31894	0.32461	0.52632	0.34847	0.56194	-6.34	-6.85	1.306
B	0.21	0.51879	0.31892	0.32574	0.53105	0.34645	0.55897	-4.99	-5.98	1.298
C	0.23	0.51842	0.31907	0.32636	0.53154	0.34595	0.55823	-4.78	-5.66	1.295
D	0.52	0.51842	0.31893	0.33679	0.54552	0.33592	0.54349	0.37	0.25	1.253
E	0.69	0.51879	0.31893	0.34266	0.55470	0.32989	0.53463	3.75	3.87	1.227
F	0.78	0.51857	0.31910	0.34556	0.56057	0.32655	0.52971	5.82	5.82	1.212
G	0.82	0.51819	0.31908	0.34694	0.56299	0.32506	0.52752	6.72	6.72	1.206
H	0.89	0.51842	0.31898	0.34897	0.56742	0.32263	0.52395	8.29	8.16	1.195
K	1.00	0.51955	0.31897	0.35084	0.57119	0.32048	0.52079	9.68	9.47	1.187

**Fig. 8** W–H plot for InGaN layers. **a** Triple-axis ω -scan and **b** triple-axis $\omega - 2\theta$ scan were measured for the symmetric (000 l) ($l = 2, 4, 6$) reflections indicated in the figure. The *lines* result from a linear fit of the data**Table 2** The mosaic properties of the GaN and InGaN epilayers that were grown on sapphire substrate are listed

Sample ID	GaN template layers					InGaN layers				
	$\alpha_{\text{twist}} (^{\circ})$	$\alpha_{\text{tilt}} \times 10^{-3} (^{\circ})$	L_{\parallel} (nm)	L_{\perp} (nm)	$\varepsilon_{\perp} (\times 10^{-4})$	$\alpha_{\text{twist}} (^{\circ})$	$\alpha_{\text{tilt}} \times 10^{-3} (^{\circ})$	L_{\parallel} (nm)	L_{\perp} (nm)	$\varepsilon_{\perp} (\times 10^{-4})$
A	–	2.5	500	26.5	-4.25	–	14.0	32.1	10.0	-1.5
B	0.13	1.0	2,250	50.0	-2.5	0.15	5.5	50.0	56.2	-2.5
C	0.25	2.8	150	32.1	-4	–	3.0	75.0	28.1	-3.0
D	0.21	1.6	6,432	34.6	-3.5	–	35.0	76.3	18.7	31.0
E	0.24	1.7	4,500	45.0	2.75	1.32	0.3	16.1	45.4	-36.7
F	0.15	2.0	4,500	28.1	-4.25	1.36	7.5	643.0	10.7	-4.5
G	0.22	1.7	6,430	32.1	-3.75	0.2	9.6	37.5	22.5	5.2
H	0.16	4.9	90	30.0	0.75	0.91	7.5	40.9	56.1	6.7
K	0.2	18	10.5	40.9	18.5	0.69	3.7	225.0	25.0	-2.0

The structural characteristics of all the samples, including the vertical coherence length, L_{\perp} lateral coherence length, L_{\parallel} vertical heterogeneous strain, ε_{\perp} parallel to the lattice vector, α_{tilt} mean tilt angle, α_{twist} mean twist angle

minor influence in this measurement case. In addition, the (0002) reflection and (hkl) reflections with either h or k non-zero orientation of our samples with triple-axis

$\omega - 2\theta$ scans, exhibit a small FWHM. The last important point is that the intrinsic width of the reflection for the crystal and the apparatus broadening for all the

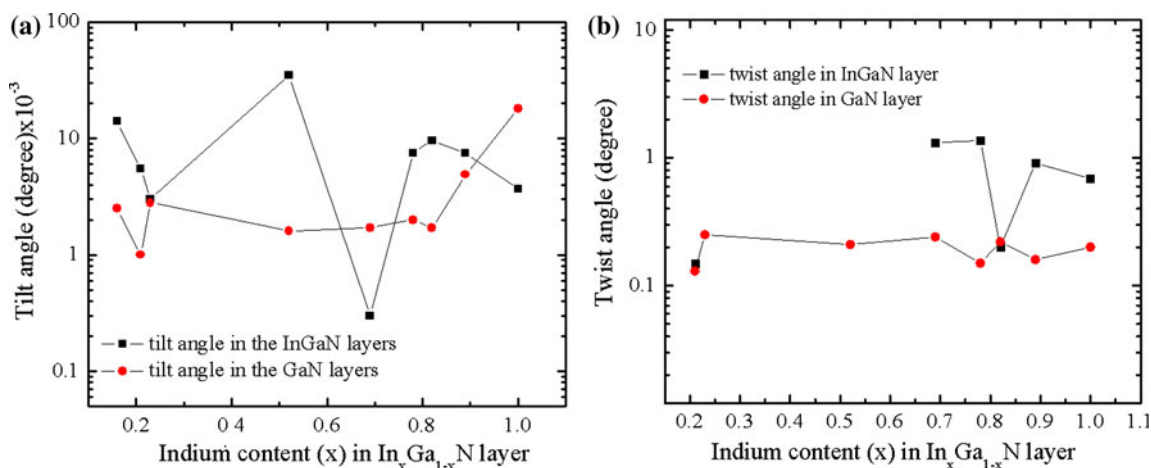


Fig. 9 Indium content dependence of the **a** tilt and **b** twist angle in GaN layers and InGaN layer for InGaN/GaN/sapphire samples

experimental reflections are negligible because these effects amount to only a few arcsec. For this reason, we can only measure the broadening that was caused by the twist using (hkl) reflections in skew geometry [9, 10, 19, 20].

Figure 10 shows the changes in FWHMs values of the ω and Φ -scans with an increasing inclination angle (χ) for the sample A. The extended FWHMs of ω and Φ -scans obtained by using the fit of Pseudo-Voigt function to the rocking curves. It can be seen in this figure that the FWHMs of ω -scans increase with the increment of χ , while the FWHM of Φ scan decrease with the increment of χ angle. Moreover, they become closer when the (12–31) reflection yields at 78.6° in χ as shown in Fig. 10. In fact, the angle χ reaches 90° when the reflection plane is perpendicular to the surface of the sample. These results showed that the rocking curve widths of ω or Φ scans for this higher χ angle are close to the twist angles. In every respect, the FWHMs of Φ -scans are larger than those of ω -scans with the change of the inclination angle χ . Therefore, the mean twist angles must be the average value of the FWHMs of ω and Φ -scans of $\chi = 78.6^\circ$.

The measured mean twist angle of the GaN template layers and InGaN epilayers are shown in Table 2. And the changes of the mean twist angle of the samples as a function of the indium content were given in Fig. 9b. The mean twist angles of the GaN template epilayer changes between 0.13° and 0.25°. It can be concluded that the mean twist angle in a GaN template are similar for all the samples. On the other hand, the mean twist angle values of the InGaN epilayers measured between 0.15° and 1.36° as shown in Table 2. The minimum mean twist angle value was obtained as 0.15° for sample B, while the maximum mean twist angle was obtained as 1.36° for sample F. Based on this observation, it can be argued that the mean twist angle of the InGaN epilayers grown on GaN template

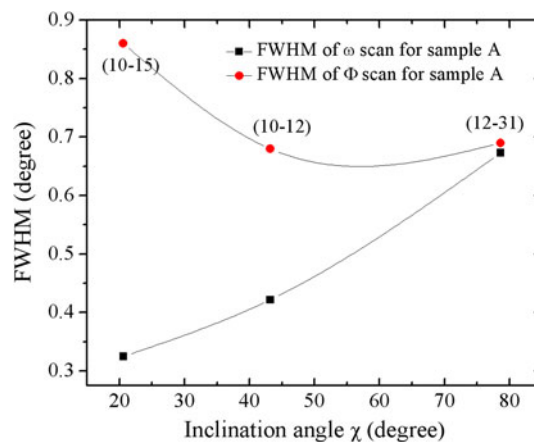


Fig. 10 FWHM of Φ and ω -scans for (hk(-h-k)l) reflections as a function of the inclination angle χ for sample A ($x = 0.16$). FWHMs of ω -scan increase with the increment of χ angle, while those of Φ scan decrease. The lines are guide for the eyes

did not strongly affect by indium content (x) in In_xGa_{1-x}N epilayers.

It is well known that the GaN based layers grown on lattice mismatched substrate, such as sapphire, SiC and Si, with two steps exhibit a high dislocation density. In this study, InGaN epilayers and GaN template were grown on sapphire substrate, which exhibit high dislocation density. There are three main types of dislocations present in InGaN epilayers and GaN template layers [7–15]; the pure edge dislocation with Burgers vector $b = \frac{1}{3}\langle 11\bar{2}0 \rangle$ ($\langle a \rangle$), the pure screw dislocation with Burgers vector $b = \langle 0001 \rangle$ ($\langle c \rangle$), and the mixed dislocation with $b = \frac{1}{3}\langle 11\bar{2}3 \rangle$ ($\langle c + a \rangle$). The edge (D_{edge}) and screw (D_{screw}) type dislocation density in the epitaxial layers can be calculated from the equation given below [9, 10, 15, 16, 18],

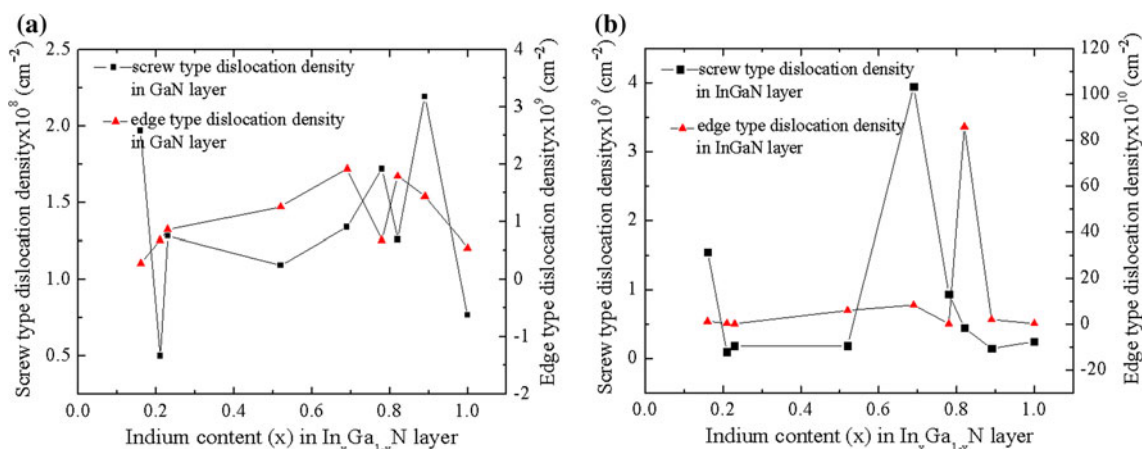


Fig. 11 Indium content dependence of the density of edge and screw type dislocation in **a** GaN layers and **b** InGaN layer for InGaN/GaN/sapphire samples

$$D_{screw} = \frac{\beta_{(0002)}^2}{9b_{screw}^2}, \quad D_{edge} = \frac{\beta_{(1012)}^2}{9b_{edge}^2}. \quad (8)$$

Where, β is the FWHM measured by HR-XRD rocking curves, and b is the Burgers vector length ($b_{screw} = 0.5185$ nm, $b_{edge} = 0.3189$ nm). And the total dislocation density (D_{dis}) of the InGaN epilayers and GaN template layers were estimated by the following equation,

$$D_{dis} = D_{screw} + D_{edge}. \quad (9)$$

The calculated edge and screw dislocation densities of the InGaN epilayers and GaN template layers are shown in Fig. 11a, b. As can be seen in Fig. 11a, the screw type dislocation density in GaN template layers changes between 5×10^7 (sample B) and 2.1×10^8 cm⁻² (sample H), but edge type dislocation densities approx. one order bigger than screw type dislocation densities and changes between 2.8×10^8 (sample A) and 1.9×10^9 cm⁻² (sample E). The calculated screw and edge type dislocation densities in InGaN epilayers were shown in Fig. 11b. In the InGaN epilayers both screw and edge type dislocation densities are approx. one order bigger than in GaN template layers. The screw type dislocation densities in the InGaN epilayers are changes between 9.8×10^7 (sample B) and 3.9×10^9 cm⁻² (sample E). On the other hand, the magnitudes of the edge type dislocation densities in InGaN epilayers were determined to range from 2.1×10^9 (sample C) to 8.6×10^{11} cm⁻² (sample G). Based on the observations in Fig. 11b, there is no systematic dependence between TD densities in InGaN epilayers and indium content (x).

4 Conclusions

In the present study, In_xGa_{1-x}N epitaxial layers, with indium content (x) of 0.16, 0.21, 0.23, 0.52, 0.69, 0.78, 0.82, 0.89 and

1.00 (InN), were grown on GaN template/sapphire substrate structure by MOCVD. The mosaic structures parameters (such as lateral and vertical coherence lengths, tilt and twist angle and heterogeneous strain) and dislocation densities (edge and screw dislocations) of the InGaN epilayers and GaN template layers were investigated by using HR-XRD measurements. Based on the HR-XRD measurements results we observed that the mosaic structures parameters, lateral and vertical coherence lengths, tilt and twist angle and heterogeneous strain of the InGaN epilayers were not strongly affected by indium content (x) in In_xGa_{1-x}N epilayers. The screw and edge type dislocation densities in InGaN epilayers were determined to range from 2.1×10^9 (sample C) to 8.6×10^{11} cm⁻² (sample G) and 2.1×10^9 (sample C) to 8.6×10^{11} cm⁻² (sample G), respectively. And there is no systematic dependence between the TD densities in InGaN epilayers and indium content (x).

Acknowledgments This work is supported by the European Union under the projects EU-METAMORPHOSE, EU-PHOREMOST, EU-PHOMÉ, and EU-ECONAM, and TUBITAK under Project Numbers 105E066, 105A005, 106E198, and 106A017. One of the authors (E. O.) also acknowledges partial support from the Turkish Academy of Sciences.

References

1. F.A. Ponce, D.P. Bour, *Nature* **386**, 351 (1997)
2. S. Nakamura, G. Fasol, *The Blue Laser Diode: GaN based Light Emitters and Lasers* (Springer, Heidelberg, 1997)
3. C. Gaquiere, S. Trassaert, B. Boudart, Y. Crosnier, *IEEE Microw. Guided. Wave. Lett.* **10**, 19 (2000)
4. X.L. Nguyen, T.N.N. Nguyen, V.T. Chau, M.C. Dang, *Adv. Nat. Sci.: Nanosci. Nanotechnol.* **1**, 025015 (2010)
5. Z.L. Li, P.T. Lai, H.W. Choi, *IEEE Photonics Technol. Lett.* **21**, 1429 (2009)
6. E. Matioli, C. Neufeld, M. Iza, S.C. Cruz, A.A. Al-Heji, X. Chen, R.M. Farrell, S. Keller, S. DenBaars, U. Mishra, S. Nakamura, J. Speck, C. Weisbuch, *Appl. Phys. Lett.* **98**, 021102 (2011)
7. F.K. Yam, Z. Hassan, *Superlattices Microstruct.* **43**, 1 (2008)

8. O. Ambacher, J. Phys. D Appl. Phys. **31**, 2653 (1998)
9. E. Arslan, M.K. Ozturk, Ö. Duygulu, A.A. Kaya, S. Ozelik, E. Ozbay, Appl. Phys. A Mater. Sci. Process. **94**, 73 (2009)
10. E. Arslan, M.K. Ozturk, A. Teke, S. Ozelik, E. Ozbay, J. Phys. D Appl. Phys. **41**, 155317 (2008)
11. J.S. Speck, S.J. Rosner, Phys. B **273–274**, 24 (1999)
12. X.H. Wu, P. Fini, E.J. Tars, B. Heying, S. Keller, U.K. Mishra, S.P. Den Baars, J.S. Speck, J. Cryst. Growth **189–190**, 231 (1998)
13. N.G. Weimann, L.F. Eastman, J. Appl. Phys. **83**, 3656 (1998)
14. G.K. Williamson, W.H. Hall, Acta Metall. **1**, 22 (1953)
15. T. Metzger, R. Höppler, E. Born, O. Ambacher, M. Stutzmann, R. Stömmer, M. Schuster, H. Göbel, S. Christiansen, M. Albrecht, H.P. Strunk, Philos. Mag. A **77**, 1013 (1998)
16. M.E. Vickers, M.J. Kappers, R. Datta, C. McAleese, T.M. Smeeton, F.D.G. Rayment, C.J. Humphreys, J. Phys. D Appl. Phys. **38**, A99 (2005)
17. V. Srikant, J.S. Speck, D.R. Clarke, J. Appl. Phys. **82**, 4286 (1997)
18. H. Heinke, V. Kirchner, S. Einfeldt, D. Hommel, Appl. Phys. Lett. **77**, 2145 (2000)
19. X.H. Zheng, H. Chen, Z.B. Yan, Y.J. Han, H.B. Yu, D.S. Li, Q. Huang, J.M. Zhou, J. Cryst. Growth **255**, 63 (2003)
20. M.K. Ozturk, Y. Hongbo, B. Sarikavak, S. Korcak, S. Ozelik, E. Ozbay, J. Mater. Sci. Mater. Electron. **21**, 185 (2010)
21. V. Holy, J. Kubena, E. Abramof, K. Lischka, A. Pesek, E. Koppensteiner, J. Appl. Phys. **74**, 1736 (1993)
22. Y.J. Sun, O. Brandt, K.H. Ploog, J. Mater. Res. **18**, 1247 (2003)
23. H. Li, Y. Luo, L. Wang, G. Xi, Y. Jiang, W. Zhao, Y. Han, Appl. Phys. Express **1**, 045004 (2008)
24. T.A. Lafford, B.K. Tanner, P.J. Parbrook, J. Phys. D Appl. Phys. **36**, A245 (2003)
25. M.S. Goorsky, B.K. Tanner, Cryst. Res. Technol. **37**, 645 (2002)
26. J. Kozłowski, R. Paszkiewicz, M. Tlaczala, Phys. Stat. Sol. (b) **228**, 415 (2001)
27. B. Heying, X.H. Wu, S. Keller, Y. Li, D. Kopolnek, B.P. Keller, S.P. DenBaars, J.S. Speck, Appl. Phys. Lett. **68**, 643 (1996)
28. Y.J. Sun, O. Brandt, T.Y. Liu, A. Trampert, K.H. Ploog, J. Blasing, A. Krost, Appl. Phys. Lett. **81**, 4928 (2002)
29. M.A. Moram, M.E. Vickers, Rep. Prog. Phys. **72**, 036502 (2009)
30. M. Schuster, P.O. Gervais, B. Jobst, W. Hosler, R. Averbek, H. Riechert, A. Iberlk, R. Stommerk, J. Phys. D Appl. Phys. **32**, A56–A60 (1999)
31. S. Pereira, M.R. Correia, E. Pereira, K.P. O'Donnell, E. Alves, A.D. Sequeira, N. Franco, I.M. Watson, C.J. Deatcher, Appl. Phys. Lett. **80**, 3914 (2002)
32. S.E. Park, O. Byungsung, C.R. Lee, J. Cryst. Growth **249**, 455 (2003)
33. P.E. Fewster, Crit. Rev. Solid State Mater. Sci. **22**, 69 (1997)
34. A.F. Wright, J. Appl. Phys. **82**, 2833 (1997)